MAGNETIC EVOKED FIELD ASSOCIATED WITH TRANSCORTICAL CURRENTS IN TURTLE CEREBELLUM

YOSHIO C. OKADA AND CHARLES NICHOLSON
Department of Physiology and Biophysics, New York University Medical Center, New York, New York 10016

ABSTRACT   The neural basis of magnetic evoked fields of the brain was studied with an isolated turtle cerebellum as a model preparation. The turtle cerebellum is a nearly flat tissue with neural processes arranged along three orthogonal axes of symmetry. According to theoretical results, this geometry should enable us to selectively measure the magnetic field due to a subpopulation of nerve cells whose longitudinal axes are perpendicular to the cerebellar surface, by simply placing the cerebellum vertically in the bath so that these cells are horizontal and by measuring the field along the rostrocaudal axis perpendicular to the longitudinal axis of these nerve cells. To elicit neural activity in these cells the dorsal midline was electrically stimulated with a bipolar electrode. Consistent with our expectations, the one-dimensional profile of the field normal to bath surface (B_z) was antisymmetrical along the rostrocaudal axis, implying that the underlying currents were transcortical. Also, the B_z field at a field extremum varied as a cosine of the orientation of the cerebellum when it was rotated about its rostrocaudal axis with the amplitude being zero when the cerebellum was horizontal. The B_z field was dipolar as judged by statistically excellent fits of the dipolar field to the one-dimensional field profile and to the distance function relating the field magnitude at an extremum to measuring distance. This was the case even for the initial component thought to be due to antidromic action currents invading the soma and dendrites of Purkinje cells. We also showed that the dipolar term of the source could be localized within 1 mm of the actual source location in most cases.

INTRODUCTION

Rather strong magnetic fields between 0.1 and 10 picotesla (pT) can be recorded during neural activity in brain tissues in vitro (Okada, 1986; Okada et al., 1986, 1987a, 1987b; Knowles et al., 1986) and in vivo (Barth et al., 1984, 1986). In our earlier studies (Okada et al., 1987b), we showed the magnetic evoked field (MEF) in isolated turtle cerebellum to be neural in origin and that a synchronous activity in a 1 mm³ of nerve tissue could lead to an MEF of as much as 0.1 pT at a source-to-field point distance of 2 cm.

Here the spatial and temporal variations of this MEF in turtle cerebellum were characterized to determine the population of nerve cells and the nature of their currents giving rise to the field. As it will be discussed below, the geometry of cellular organization in turtle cerebellum makes it an ideal model for studying the relationship between the MEF and the underlying neural currents in brain tissues. We hope that understanding of this relationship will be valuable for interpretation of the human magnetoencephalograms.

In our in vitro preparation the whole cerebellum is removed from the rest of the turtle brain and suspended in a large bath of physiological saline. Thus the MEF outside the bath can be unambiguously identified with currents in the cerebellum without complications arising from the presence of other parts of the brain and structures such as

the skull as in the case of in vivo and intact preparations (Fig. 1 *A*).

Furthermore, the gross shape and cellular organization of the cerebellum enable us to selectively measure the MEF due to a subset of neural currents oriented along the principal core conductors (namely Purkinje cells) whose longitudinal axes are perpendicular to the cerebellar surface. The turtle cerebellum is a lissencephalic oblate spheroid and becomes nearly flat when placed on a supporting net in the bath (Figs. 1, *B* and *C*). The nerve cells and their processes (dendrites and axons) are arranged along three orthogonal axes of symmetry. Purkinje cells, granule cells, and Golgi cells have their longitudinal axes oriented perpendicular to the cerebellar surface, along the ventrodorsal (y) axis. There are also radial ependymal astrocytes which have their somas at the ventral surface and their processes running all the way to the dorsal surface. The branched axons of granule cells, the parallel fibers, run perpendicular to these cell processes, along the medial-lateral (z) axis in the molecular layer. In higher species, the third axis, the rostrocaudal (x) axis, is occupied by the axons of inhibitory interneurons (Basket cells) (Ramón y Cajal, 1911; Eccles et al., 1967), but in the turtle cerebellum these are not well developed (Larsell, 1932). Another group of interneurons called stellate cells are present in the molecular layer, but most likely do not produce significant magnetic fields because of their so-
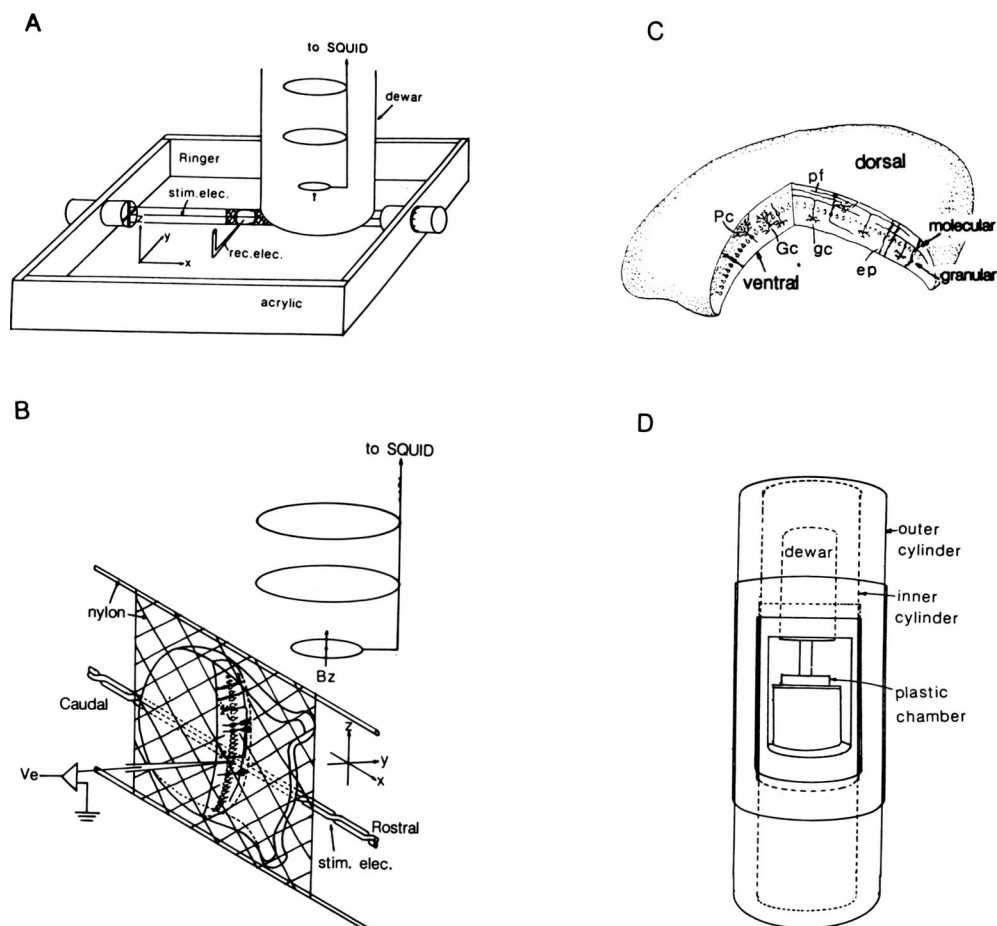
A

C

called closed field configuration (Lorente de No, 1947). The MEF of the cerebellum then may be due to a mixture of currents in these three populations of neural elements. However, its cellular organization enables us to selectively measure the MEF due to a subpopulation of nerve cells whose longitudinal axes are oriented perpendicularly to the cerebellar surface, by simply orienting the cerebellum vertically with Purkinje cells horizontal and parallel fibers vertical and measuring the component of the MEF normal to bath surface (Bz) along the rostrocaudal (*x*) axis perpendicular to the longitudinal axis of Purkinje cells (Fig. 1 *B*). In this case the Bz field should be solely due to the horizontal currents perpendicular to the cerebellar surface (Geselowitz, 1970; Grynszpan and Geselowitz, 1973; Cohen and Hosaka, 1976; Cuffin and Cohen, 1979). The vertical component of cerebellar currents should not directly produce any MEF outside the bath because of Ampere's law.

The turtle cerebellum is also useful for a practical reason. It can tolerate anoxia well (Lutz et al., 1980; Sick et al., 1982). Thus the entire cerebellum can be kept physiologically functioning for more than one day by simply keeping it in an oxygenated Ringer solution (Chan and Nicholson, 1986). Because measurements of the MEF

usually take at least several hours, this tolerance for anoxia simplifies our interpretation of MEF.

The specific purposes of this study were then: (*a*) to verify the theoretical prediction that the MEF in our preparation should be due to currents oriented perpendicularly to the cerebellar surface, (*b*) to infer the nature of the underlying current based on a quantitative characterization of the MEF, and (*c*) to evaluate the accuracy of localizing the active tissue in three dimensions based on the measured MEF.

METHODS

The experimental preparation will be described in some detail here, because it has not been done so before (see Fig. 1).

Animal Preparation. The brain of the red-eared turtle (*Pseudemys scripta elegans*) was removed rapidly after decapitation and craniotomy and placed in a Ringer solution (100 mM NaCl; 5 mM KCl; 40 mM NaHCO$_3$; 3.5 mM CaCl$_2$; 3.5 mM MgCl$_2$; 20 mM glucose). Then, the whole cerebellum was removed from the rest of the brain by cutting it just caudal to the optic tectum and below the cerebellar peduncle. The isolated cerebellum was subsequently placed in an acrylic chamber (15 × 15 × 4.5 cm) filled with 600 ml of Ringer solution continuously oxygenated with 95% O$_2$ and 5% CO$_2$ (Fig. 1 *A*). The cerebellum was supported with a nylon net on its ventral side and a pair of twisted, enamel-coated silver wires touching the dorsal midline for stimulation. The cerebellum could be continuously rotated about the axis of the

stimulating electrode which corresponded to the rostrocaudal axis of the cerebellum.

Stimulus. Neural activity was evoked in the cerebellum by stimulating the dorsal midline with a brief 30–60–μs monopolar pulse applied every 2 s through the pair of stimulating electrodes. The 1 mm of enamel insulation apposing the dorsal pial surface was removed for stimulation (Fig. 1 *B*).

Signal Recording. The Bz field was measured on bath surface along the rostrocaudal (x) axis of the cerebellum (Fig. 1 *B*). The detector consisted of an asymmetric second-order gradiometer coupled inductively to a dc-SQUID (Superconducting Quantum Interference Device) made by Biomagnetic Technologies, Inc., San Diego, CA. The gradiometer was made of three sets of coaxial coils with a bottom, pickup coil having a diameter of 10 mm with two upper cancellation coils of 20 mm in diameter spaced 40 mm apart. The distance between the pickup coil and the outer surface of the tail section of the cryogenic dewar housing the gradiometer was 13 mm, as determined by a search coil and by an x-ray picture. Using these two independent methods, we also determined the center of the pickup coil relative to the center of the dewar tail section. The field sensitivity of the detecting system was 12–15 fT$_{rms}$/Hz$^{1/2}$. The output of the detector was amplified and filtered between 0.5 Hz and 2 kHz with a Butterworth filter having an amplitude roll-off of 24 dB/octave (Bioengineering Technologies, Inc., Thornwood, NY), then digitized at 5 kHz with an 11/23+ computer (MDB Inc., Los Angeles, CA) equipped with a 35-kHz ADC-DAC card (Data Translation, Cambridge, MA) for an on-line averaging over a duration of 51.2 ms, including 5 ms during the prestimulus period. The stimulus artifact was reduced by placing the detecting coil symmetrically over the stimulating electrode and by using a buckout coil several centimeters away from the detecting coil. The buckout coil was connected in series with the stimulating electrode, so that it could be oriented in such a way as to null the stimulus artifact.

The extracellular potential (Ve) was measured simultaneously with the magnetic signal on each stimulus epoch with a glass mciropipette of 2–5 μm in tip diameter filled with 1 M sodium acetate, referred to the potential at the ground electrode placed in one corner of the acrylic chamber. The ground electrode was made of a Pasteur pipette filled with 1 M KCl in 3% agar having a Ag-AgCl coated silver wire as the lead. The Ve in this study was mostly monitored in the molecular layer to check the response of the cerebellum to the stimulation. The micromanipulators used for Ve recording (Narishige MO-103 and MM-3) were modified by replacing all ferromagnetic materials with nonferrous materials to eliminate the vibration noise that would be introduced into the output of the magnetic detector. The electric signal was preamplified ($\times$5) by an FET headstage (Bioengineering Technologies, Inc., Thornwood, NY) and then further amplified and filtered with the Butterworth filter identical to that used for the magnetic recording, having a bandwidth of 0.5 Hz to 2 kHz, and digitized at 5 kHz for signal averaging.

Both raw and averaged signals were monitored on oscilloscopes in real time. The sensitivity of the magnetic detector was sufficiently high for seeing the unaveraged magnetic signal. A complete replication was obtained at least three times for each set of measurements.

Magnetic Shielding. The entire experiment was carried out in a magnetically shielded chamber to reduce rf interference, line frequency noise, and low-frequency magnetic noise below 1 Hz (Fig. 1 *C*). The rf and line-frequency noise in our laboratory turned out to be too high to carry out measurements in a nonshielded environment. We also found it necessary to reduce the low frequency noise to a level below that which could be achieved with the second order gradiometer configuration to carry out measurements of dc and very slowly varying fields (Okada, 1986, Okada et al., 1986, 1987a).

The shield consisted of two concentric cylinders with caps on both ends, made of 1-mm-thick permalloy with a permeability of 50,000–500,000 (Amuneal, Philadelphia, PA). The inner and outer cylinders were both 196.0 cm high and 42.7 cm and 68.1 cm in diameter, respectively. Each cylinder had a window cut in its body. Its dimensions were 38.5 × 47.5 cm and 51.0 × 57.0 cm, respectively, for the inner and outer cylinders. These windows were opened during the preparation of an experiment and closed during measurements. The windows were opened and closed by rotating a shorter cylinder (102 cm in height) with a window of the same dimension. Their diameters were 43.1 and 68.5 cm, leaving a 1-mm air gap between the long and short cylinders. All the tubings were inserted into the chamber through either the top (9 cm diameter) or bottom hole (8 cm diameter). The dc-shielding factor along the vertical axis at the center of the chamber was 10,000, the field amplitude being on the order of 5 nT when measured with a fluxgate magnetometer (MF5000, Automation Industries, Danbury, CT).

RESULTS

Fig. 2 shows the one-dimensional profile of the Bz field along the rostrocaudal (x) axis at a height of 17 mm from the cerebellar midline. These waveforms are averages of responses from 100 stimulus epochs. As in our earlier studies (Okada, 1986; Okada et al., 1986, 1987a), the temporal waveform of the field consisted of an initial biphasic spike with a peak latency of 1.0 to 1.2 ms and a slower component lasting 5–10 ms. However, a slower third component having a latency of ~15 ms was barely noticeable in the present records. The polarities of these components were such that the current underlying the peak of the initial biphasic component (labeled component *a* in Fig. 2; 1.0 ms latency) was directed from the ventral to the dorsal side of the cerebellum. So was the second component (labeled component *b*). We will relate the underlying
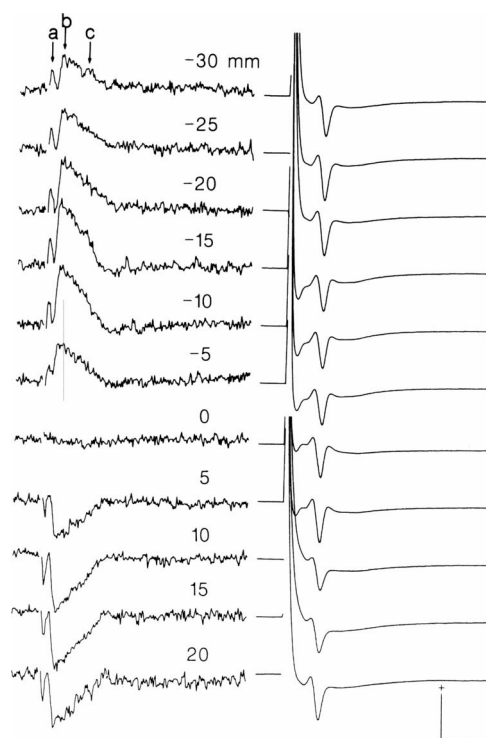

FIGURE 2 Variation of the magnetic field (Bz) along the rostrocaudal direction (x-axis) 17 mm above (z = 17 mm) the cerebellar midline. + = rostral. The dorsal surface faced the +y-axis. (*Left*) Magnetic field (Bz). (*Right*) Extracellular potential (Ve). Calibration, 1 pT/2 mV/10 ms. Positive Bz is directed outward from the bath as in all the data presented in this article.

currents to physiological events in the Discussion. These records clearly indicate that the Bz field was antisymmetrical about the center of the cerebellum.

The Ve measured in the molecular layer demonstrates that the preparation was physiologically stable during the sequential measurements of the Bz field. The relatively strong stimulus artefact in these records is due to the fact that the recording electrode was placed in the superficial molecular layer close to the 1-mm long pair of stimulating electrode positioned over the dorsal midline. The major components of the Ve consisted of a diphasic, positive–negative waveform followed by a slower negativity normally seen in the field potential measured in the molecular layer in response to a superficial stimulation (Eccles et al., 1966d). The initial positive–negative complex reflects the action potentials generated by direct stimulation of the parallel fibers, and the slower negativity largely reflects postsynaptic dendritic potentials of Purkinje cells generated by the parallel fibers.

The difference in waveform between the MEF and Ve is due to differences in the currents giving rise to these signals. The Ve, on the one hand, is a weighted sum of potentials produced by neural elements in a small region around the recording electrode tip located in the molecular layer (Nicholson, 1973). Thus the latency of the response varies with the position of the recording electrode relative to the stimulating electrode (Eccles et al., 1966d). The MEF measured a few centimeters away from the brain tissue, on the other hand, is a vector sum of the fields produced by currents in the entire active tissue. Thus, its temporal waveform should be dominated by strongest currents in the tissue and its latency depends on a weighted average of latencies of currents in the entire active tissue. We will consider this issue further in the Discussion.

Fig. 3 shows the variation of the Bz field amplitude as a function of the distance along the rostrocaudal axis for three components of the field (indicated by arrows) in Fig. 2. The smooth curves indicate the theoretical field profiles for the dipole term of the current source. Each fit was obtained with a least-squares method, estimating the depth, x-coordinate, and moment of the dipole from the data while keeping the remaining two parameters, y-coordinate and orientation on the x-y plane, fixed at zero. The calculation of theoretical field took into account the coil geometry of the sensor, using a lead field method (Jackson, 1962; Plonsey, 1972; Williamson and Kaufman,
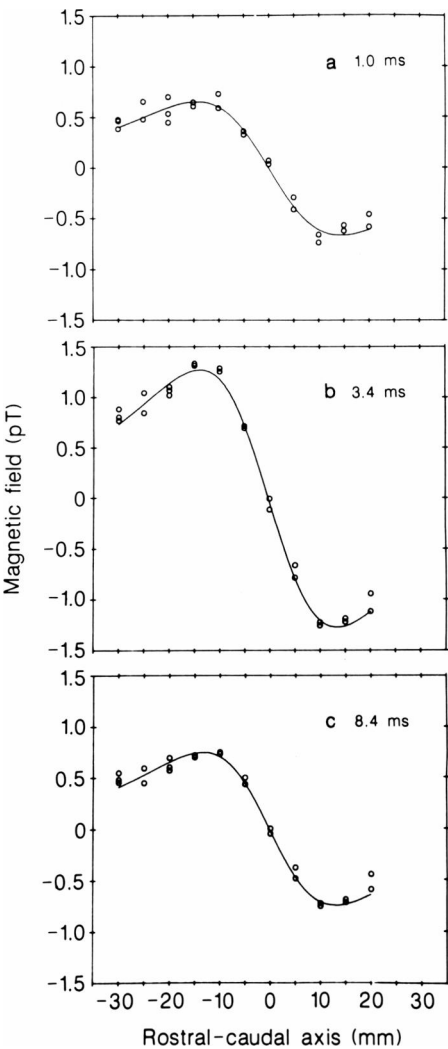
FIGURE 3   One-dimensional profile of the Bz along the rostrocaudal axis for components a, b, and c of the MEF shown in Fig. 2. Latencies of the three components are indicated in each panel. (Open circles) Data. (Curves) Theoretical fields for a current dipole. See the text for details.

1981). On visual inspection the fits appear to be quite good.

Table I presents values of the free parameters of the best-fitting dipole, along with some statistics for the goodness of fit. The values of source location along the x-axis (X) and depth are with respect to the center of the active tissue determined physically. In five out of six cases the

TABLE I
PARAMETERS OF THE EQUIVALENT CURRENT DIPOLE ESTIMATED FROM THE 1-D FIELD PROFILE

Time	X	Depth	Q	Error$_{fit}$	Error$_{data}$	Chi^2	Error$_{residual}$
ms	mm	mm	nA · m				
1.0	0.0 ± 0.4	−1.8 ± 0.3	9.1 ± 0.3	90	81	25	39
3.4	−0.3 ± 0.2	−0.6 ± 0.1	15.5 ± 0.2	89	68	34	58
8.4	−0.3 ± 0.3	0.3 ± 0.2	8.3 ± 0.2	75	58	33	48

errors were <0.6 mm. Thus it was possible in this experiment to localize the x- and z-coordinates of the dipole term with an accuracy of better than 1 mm. The dipole moment was ~10 nA · m for the active tissue involved. The extent of the active tissue was found to be ~10 mm² in surface area in an experiment where the laminar profile of the Ve was measured along two tracks, one on each side of the stimulating electrode. Thus the field was associated with neural currents corresponding a dipole moment of ~1 nA · m/mm². Statistically the data could be satisfactorily accounted for by the dipole component of the current generator (χ^2 [df = 20] = 25–33, $P > 0.01$). The error of fit defined as the standard deviation of theoretical values from the data points was 75–90 fT, whereas the standard deviation of the data points about their means was on the average 58–81 fT. The error in the fit unaccounted for by the variability in the data was 39–58 fT, assuming statistical independence of the error terms.

The one-dimensional field profile implies that the MEF was due to currents perpendicular to the cerebellar surface. To verify this conclusion, we next measured the Bz field at a field extremum as a function of orientation of the cerebellum about the rostrocaudal axis. If the field shown in Fig. 1 were indeed due to currents perpendicular to the cerebellar surface, then the amplitude of the Bz field at an extremum should vary as a cosine of the orientation of the cerebellum. As shown in Fig. 4, the cerebellum viewed from its rostral side was rotated in this experiment from 0 to 180° in 20° steps and the Bz field was measured 13 mm rostral to and 17 mm above the cerebellar center. The first five waveforms from the top are averages of responses in 200 epochs each, whereas the remaining waveforms are averages of 400 epochs each. The record for 40° orientation contains some line frequency noise. Clearly, the waveforms were mirror-images of each other about 90° and the field amplitude was zero at 90°.

Fig. 5 shows the variation of field amplitude as a function of orientation of the cerebellum for the three components indicated by arrows in Fig. 4. The smooth curves are the cosine functions fitted to the data with a

FIGURE 4   Variation of the Bz at a field extremum $(x, y, z) = (13, 0, 17$ mm) as a function of orientation of the cerebellum. The cerebellar orientation, as viewed from its rostral side, is shown next to some traces. Calibration, 1 pT/5 ms. The three components with latencies of 1.0, 3.0, and 5.2 ms, indicated by arrows, are analyzed in Fig. 5.

least-squares method. Two parameters of the cosine function, orientation offset and maximum amplitude, were estimated from the data.

As shown in Table II, the result of the fit was consistent with the conclusion that the field was due to currents perpendicular to the cerebellar surface. The orientation offset (theta) was $\leq 7°$. The error of fit was 121–161 fT. This amount of error was statistically indistinguishable

FIGURE 5   Comparison of the measured and theoretical orientation function for three time components of the responses shown in Fig. 4. (Open circles) Data. (Curves) $B_{max,z}$, cos $(\phi + \theta)$, ϕ, θ in degrees, where $B_{max,z}$ and θ were determined from data.

TABLE II

PARAMETERS OF THE COSINE FUNCTION ESTIMATED
FROM THE ORIENTATION FUNCTION

Time	Theta	B_{max}	$Error_{fit}$	$Error_{data}$	Chi^2	$Error_{residual}$
ms	degree	pT				
1.0	0 ± 8	1.34 ± 0.08	161	230	7	NA
3.0	−5 ± 3	2.02 ± 0.04	139	122	19	67
5.2	−7 ± 3	1.38 ± 0.03	121	84	31	87

from the error due to the variability of the data (χ^2 [df = 15], $P \geq 0.01$).

In the experiment shown in Fig. 2 we found that the Bz field was dipolar. To validate this result, we measured the amplitude of the Bz at a field extremum as a function of distance z between the center of the cerebellum and the pickup coil. For each height, the detector position along the x-axis was adjusted to measure the Bz field at its extremum, according to the rule given in Williamson and Kaufman (1981), so that the amplitude should decrease as $1/z^2$ for a dipolar field. The averaged waveforms in Fig. 6 indicate that the waveform remained virtually invariant but the amplitude decreased with the distance. The records are based on 200 epochs for $z = 17–34$ mm and 300 for $z = 43$ mm and 400 for $z = 54$ mm.

Fig. 7 clearly shows that the field amplitude at an extremum decreased as a current dipolar field for the three time components indicated by the arrows in Fig. 6. In Fig. 7 A the field amplitude is plotted against distance z in a log–log form. The circles are the measured values. The smooth curves are the theoretical values for a best-fitting current dipole that would be sensed by the gradiometer used in our experiments. The curves are nonlinear, instead of straight lines with a slope of −2 for an ideal detector, because of two factors. The finite pickup coil diameter of 10 mm, on one hand, reduces the field amplitude sensed by
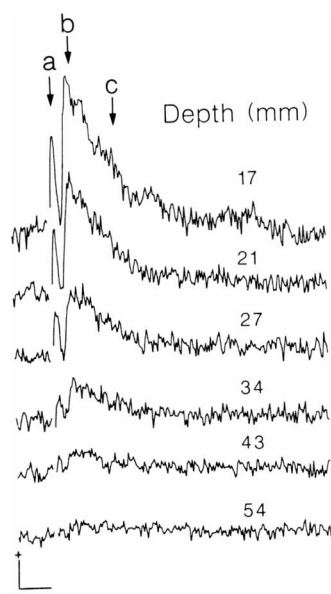

FIGURE 6 Variation of the Bz as a function of distance between the cerebellar midline and the pickup coil. The Bz was measured at a field extremum appropriate for each distance $(x, y, z) = (-z/\sqrt{2}, 0, z)$. Calibration, 250 fT/5 ms.
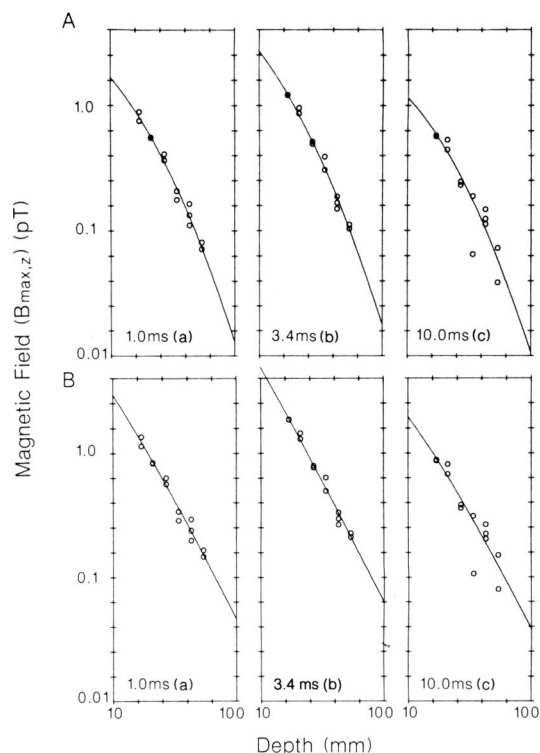

FIGURE 7 Comparison of the measured and theoretical distance functions in a log–log plot for three components of the responses (labeled a, b, and c with latencies of 1.0, 3.4, and 10.0 ms) in Fig. 6. (A) Circles, raw data; curves, theoretical values for best-fitting current dipoles that would be sensed by the gradiometer used in this study. (B) Circles, measured Bz amplitudes corrected for the coil geometry of the gradiometer (removing the distortions introduced by the finite pickup coil diameter and baseline); curves, theoretical values of the best-fitting dipoles that would be sensed by an ideal point magnetometer with an infinitesimally small pickup coil and without any cancellation coils.

this gradiometer when the distance is less than ~20–30 mm. The finite baseline (coil-to-coil separation), on the other hand, reduces the field amplitude sensed by the detector when z is more than the baseline (i.e., 40 mm). The fit was carried out by estimating the depth (z) and moment (Q) of the current dipole from the data, while keeping fixed the x- and y-coordinates and the orientation of the dipole on the x-y plane to all zero.

Fig. 7 B show the same data and functions after correcting for the coil geometry of the detector. That is, we used the theoretical and experimental values in Fig. 7 A to compute the field amplitudes that would have been sensed if we used a point magnetometer with an infinitesimally small pickup coil without any cancellation coils. To correct each data point, we first estimated the dipole moment associated with the data point from the measured value of the field and a dipole located at the position found for the dipole in Fig. 7 A. The dipole moment was then converted to a field value using Biot-Savart law. The corrected theoretical function was obtained similarly from the best-fitting parameters of the dipole found in Fig. 7 A. It can be seen that the theoretical curves are now nearly straight.

The remaining nonlinearity is due to the offset z_0 of the parameter z which was left as a free parameter in the above fit. A least-squares fit of a straight line to the corrected data yielded a slope of -2.0 ± 0.1 for the 1.0 and 3.4 ms components and a slope of -2.0 ± 0.3 for the 10.0 ms component.

A statistical evaluation of the goodness of fit shown in Table III indicates that it was within the variability of the data (χ^2 [df = 10] = 9.5–16.2, $P > 0.05$). However, the estimated location of the depth of the dipole term deviated from the physical center of the active tissue by as much as -4.1 mm, much larger than the result obtained for the one-dimensional profile. The deviation was not consistent across replications, so that it is premature to attach significance to the sign of the deviation. These relatively large deviations are perhaps due to the fact that the depth parameter z_0 was strongly determined by the measured field values at close distances rather than by the entire set of data points as in the case of the one-dimensional field profile. The dipole moment was again ~ 10 nA $\cdot$ m.

DISCUSSION

The above results demonstrate that the MEFs in our experiments were indeed due to currents oriented perpendicularly to the cerebellar surface. The Bz field was antisymmetrical along the rostrocaudal axis. Also, its amplitude varied as a cosine of the orientation of the cerebellum. The orientation effect emphasizes that the Bz field was due to currents tangential to the bath surface.

The relative simplicity of the measured field was achieved by taking advantage of some of the inherent properties of magnetic field together with a proper choice of the method of stimulation, recording, and preparation. One may expect a dorsal stimulation to produce currents in parallel fibers and possibly in the afferent and efferent fibers running rostrocaudally as well as in Purkinje cells and others whose axes are perpendicular to the cerebellar surface. If all these currents were to contribute to the MEF, it would be difficult to interpret the result in terms of the underlying current. Thus the above experiments were designed to selectively measure the MEF due to currents along only one axis. To minimize the possible contribution of parallel fibers the stimulating electrode was placed along the dorsal midline. This symmetrical stimulation should have made the field due to action currents in parallel fibers predominantly octopolar, because action

currents should presumably generate quadrapolar fields (Wikswo, 1983; Tripp, 1981) and such a stimulation should generate action currents travelling away from the midline. The measurement of the MEF over the rostrocaudal axis enabled us to select the fields due to the dipolar term of transcortical currents, because the quadrapolar term of such currents or the currents produced by the afferent and efferent fibers along the rostrocaudal axis should generate fields that are shaped like a four-leaf clover with null field along the rostrocaudal axis. The one-dimensional field profile and the orientation function supported our expectation that the MEF along the rostrocaudal axis should be due to transcortical currents.

Having verified that the MEF was due to transcortical currents, we can infer the nature of this current underlying the measured field. We expected the stimulation of the superficial dorsal surface to excite parallel fibers which in turn excite dendrites of Purkinje cells. The extracellular potential (Ve) recorded in the molecular layer (Fig. 2) showed that indeed this pattern of activation occurred in our experiment, because the Ve was similar in waveform to those classically observed (Eccles et al., 1966d). If these were the only elements activated by the stimulus, the corresponding MEF measured over the rostrocaudal (x) axis should have been due to transcortical currents directed from the dorsal to the ventral side. However, the underlying current of the measured MEF was directed from the ventral to the dorsal side. This implies that the dorsal stimulation activated not only parallel fibers but also other elements. It is known that when the stimulus strength is increased, axons of Purkinje cells are antidromically excited and the mossy and climbing fibers are orthodromically excited (Eccles et al., 1966d). These excitations can lead to intracellular currents directed from the ventral to the dorsal side, because they give rise to current sinks ventral to the superficial molecular layer. Consistent with the above conjecture, an ongoing study indicates that a dorsal-to-ventral current can be observed with a peak latency of ~ 16 ms when the stimulus is relatively weak but, as the stimulus strength is increased, the ventral-to-dorsal currents with shorter latencies become predominant. It appears then that in the present series of experiments the stimulation activated the ventral as well as the dorsal side of the cerebellum and that it activated generators of strong currents directed from the ventral to the dorsal side.

It is possible to infer the nature of these strong currents directed dorsally on the basis of properties of the MEF we have found thus far and earlier electrophysiological studies. Judging from the latencies and field polarities, it appears that the initial, fast component was in large part due to the antidromic action current invading the soma and dendrites of Purkinje cells (Eccles et al., 1966a and b). Consistent with this inference, this component was only slightly sensitive to Mn^{2+} added to the bath, relative to the later components which were virtually eliminated by the same concentration of Mn^{2+} (Okada et al., 1987b). The

TABLE III
PARAMETERS OF THE EQUIVALENT DIPOLE
ESTIMATED FROM THE DISTANCE FUNCTION

Time	Depth	Q	$Error_{fit}$	$Error_{data}$	Chi^2	$Error_{residual}$
ms	mm	nA $\cdot$ m				
1.0	-2.7 ± 0.3	12.8 ± 0.4	41	42	9.5	NA
3.4	-1.5 ± 0.2	17.1 ± 0.3	45	36	15.5	27
10.0	-4.1 ± 0.4	10.8 ± 0.4	55	43	16.2	34

size of the extracellular and intracellular potentials produced by antidromic currents in Purkinje cells (Eccles et al., 1966a and b) strongly point to this action current as the source of the initial component of the MEF. This conclusion implies that it is possible to detect action currents with the magnetic technique in in vitro preparations. Evidently, our data suggest that the antidromic action current invading Purkinje soma and dendrites contains a significant dipolar component, that is the spatial gradient of the action potential is probably asymmetric with the accompanying internal longitudinal current oriented primarily from the soma to the dorsal end of the apical dendrites. The second portion of this fast biphasic spike may represent the field due to the repolarization of the antidromic potential.

The second component (3–6 ms latency) is probably a mixture of various postsynaptic currents. The direction of the field indicates that the predominant current was directed from the ventral to the dorsal side. Our conjecture is that this strong source of current is the postsynaptic current produced by inputs from the climbing fibers. Kunzle (1985) has recently shown that climbing fibers terminate only on the lower third of the Purkinje cell dendritic tree. The selective stimulation of the climbing fibers in turtle (Bantli, 1974) produces a laminar profile of extracellular potential with negativity in the granular and Purkinje cell layers and also in the deep part of the molecular layer. This laminar profile implies that the internal longitudinal current was directed from the ventral to the dorsal side. The climbing fiber activation produces a large intra- and extracellular potential (Eccles et al., 1966e). The large number of synaptic connections made by each climbing fiber onto its target Purkinje cell (Llinas et al., 1969) seems to support a strong internal longitudinal current. The postsynaptic currents in granule cells along the depth of the cerebellum are in the form of action currents in the ascending axons. These action currents give rise to a triphasic extracellular potential in cats (Eccles et al., 1966c). Thus their MEFs might be quadrapolar without a significant dipolar term. The other currents in the neurons should be oriented from the dorsal to the ventral side.

Finally, the present study showed that the magnetic field measured ~2 cm from a brain tissue can be used to localize the active tissue within 1 mm of its actual location along the rostrocaudal axis and depth. This level of accuracy was obtained here partly because of the simplicity of the experimental arrangement afforded by the isolated cerebellar preparation. Nevertheless, this localization demonstrates that the magnetic technique can achieve an accuracy of better than 1 mm under certain ideal conditions. One should bear in mind, however, that the accuracy of localization may degrade in more complex cases due to the presence of probe positioning error, multiple sources, and other factors. It should also be noted that the accuracy of localization referred to here pertains to localization of the center of activity. We did not address the question of determining the size of active tissue directly from measured MEF, because the size of active tissue (less than ~10 mm^2) was too small for such an estimation under the conditions of measurements that were in effect in our present study (Okada, 1985).

REFERENCES

Bantli, H. 1974. Analysis of differences between potentials evoked by climbing fibers in cerebellum of cat and turtle. *J. Physiol. (Lond.).* 37:573–593.

Barth, D. S., W. Sutherling, and J. Beatty. 1984. Fast and slow magnetic phenomena in focal epileptic seizures. *Science (Wash. DC).* 226:855–857.

Barth, D. S., W. Sutherling, and J. Beatty. 1986. Intracellular currents of interictal penicillin spikes: evidence from neuromagnetic mapping. *Brain Res.* 368:36–48.

Chan, C. Y., and C. Nicholson. 1986. Modulation by applied electric fields of Purkinje and stellate cell activity in the isolated turtle cerebellum. *J. Physiol. (Lond.).* 371:89–114.

Cohen, D., and H. Hosaka. 1976. Magnetic field produced by a current dipole. *J. Electrocardiol. (San Diego).* 9:409–417.

Cuffin, B. N., and D. Cohen. 1979. Comparison of the magnetoencephalogram and electroencephalogram. *Electroenceph. Clin. Neurophysiol.* 47:132–146.

Eccles, J. C., M. Ito, and J. Szentagothai. 1967. The Cerebellum as a Neuronal Machine. Springer-Verlag, New York.

Eccles, J., R. Llinas, and K. Sasaki. 1966a. The action of antidromic impulses on the cerebellar Purkinje cells. *J. Physiol. (Lond.).* 182:316–345.

Eccles, J., R. Llinas, and K. Sasaki. 1966b. Intracellularly recorded responses of the cerebellar Purkinje cells. *Exp. Brain Res.* 1:161–183.

Eccles, J., R. Llinas, and K. Sasaki. 1966c. The mossy fiber-granule cell relay of the cerebellum and its inhibitory control by Golgi cells. *Exp. Brain Res.* 1:82–101.

Eccles, J., R. Llinas, and K. Sasaki. 1966d. Parallel fiber stimulation and the responses induced thereby in the Purkinje cells of the cerebellum. *Exp. Brain Res.* 1:17–39.

Eccles, J., R. Llinas, K. Sasaki, and P. E. Voorhoeve. 1966e. Interaction experiments on the responses evoked in Purkinje cells by climbing fibers. *J. Physiol. (Lond.).* 182:297–315.

Geselowitz, D. B. 1970. On the magnetic field generated outside an inhomogenous volume conductor by internal current sources. *IEEE (Inst. Electr. Electron. Eng.) Trans. Biomed. Eng.* MAG-6:346–347.

Grynszpan, F., and D. B. Geselowitz. 1973. Model studies of the magnetocardiogram. *Biophys. J.* 13:911–925.

Jackson, J. D. 1962. Classical Electrodynamics. John Wiley & Sons, New York. 142.

Knowles, W. D., C. D. Tesche, L. Krusin-Elbaum, and R. D. Traub. 1986. SQUID measurements of magnetic fields generated by the *in vitro* hippocampal slice. *Soc. Neurosci. Abstr.* 12:850.

Kunzle, H. 1985. Climbing fiber projection to the turtle cerebellum: longitudinally oriented terminal zones within the basal third of the molecular layer. *Neuroscience.* 14:159–168.

Larsell, O. 1932. The cerebellum of reptiles: chelonians and alligator. *J. Comp. Neurol.* 56:299–345.

Llinas, R., J. Bloedel, and D. Hillman. 1969. Functional characterization of neuronal circuitry of frog cerebellar cortex. *J. Neurophysiol. (Bethesda).* 32:847–870.

Lorente de No, R. 1947. Action potential of the motoneurons of the hypoglossus nucleus. *J. Cell. Comp. Physiol.* 29:207–287.

Lutz, P. L., J. C. LaManna, M. R. Adams, and M. Rosenthal. 1980. Cerebral resistance to anoxia in the marine turtle. *Respir. Physiol.* 41:241–251.

Nicholson, C. 1973. Theoretical analysis of field potentials in anisotropic ensembles of neural elements. *IEEE (Inst. Electr. Electron. Eng.) Trans. Biomed. Eng.* BME-20:278–288.

Okada, Y. C. 1985. Discrimination of localized and distributed current dipole sources and localized single and multiple sources. *In* Biomagnetism. H. Weinberg, G. Stroink, and T. Katila, editors. Pergamon, New York. 266–272.

Okada, Y. C. 1986. Physiological basis of magnetoencephalography. *Ann. Biomed. Eng.* 14:84.

Okada, Y. C., M. Lauritzen, and C. Nicholson. 1986. Evoked magnetic field detected from isolated cerebellum *in vitro* during Purkinje cell activity and spreading depression. *Soc. Neurosci. Abstr.* 12:1132.

Okada, Y. C., M. Lauritzen, and C. Nicholson. 1987a. Source models and physiology. *Phys. Med. Biol.* 32:43–51.

Okada, Y. C., M. Lauritzen, and C. Nicholson. 1987b. Magnetic field associated with neural activities in an isolated cerebellum. *Brain Res.* 412:151–155.

Plonsey, R. 1972. Capability and limitation of electrocardiography and magnetocardiography. *IEEE (Inst. Electr. Electron. Eng.) Trans. Biomed. Eng.* BME-19:239–244.

Ramón y Cajal, S. 1911. Histologie du Systéme Nerveux de l'Homme et des Vertébrés. Maloine, Paris.

Sick, T. J., M. Rosenthal, J. C. LaManna, and P. L. Lutz. 1982. Brain potassium ion homeostasis, anoxia, and metabolic inhibition in turtles and rats. *Am. J. Physiol.* 43:R281–R288.

Tripp, J. H. 1981. Biomagnetic fields and cellular current flow. *In* Biomagnetism. S. N. Erne, H.-D. Hahlbohm, and H. Lubbig, editors. de Gruyter, New York. 207–215.

Wikswo, J. P., Jr. 1983. Cellular action currents. *In* Biomagnetism. S. J. Williamson, G-L. Romani, L. Kaufman, and I. Modena, editors. Plenum Publishing Corp., New York. 173–207.

Williamson, S. J., and L. Kaufman. 1981. The magnetic field of the cerebral cortex. *In* Biomagnetism. S. N. Erne, H.-D. Hahlbohm, and H. Lubbig, editors. de Gruyter, New York. 353–402.